communications engineering

A Nature Portfolio journal

Article

https://doi.org/10.1038/s44172-025-00442-1

Early warning of thermal runaway based on state of safety for lithium-ion batteries

Xin Gu[1,2], Yunlong Shang[1] ✉, Jinglun Li[1,2], Yuhao Zhu[1], Xuewen Tao[1], Hao Geng[1], Zhen Zhang[1] & Chenghui Zhang[1] ✉

Ensuring the safety of lithium-ion power batteries is the primary prerequisite for developing electric vehicles and energy storage systems. The conventional method relies on temperature parameters and only qualitatively assesses the state of safety (SOS), which reduces the warning time of the battery management system (BMS). Here we present a thermal runaway warning method based on SOS. Specifically, we analyze the strain evolution trend of thermal runaway under different abuse conditions and propose the strain trigger point for thermal runaway. Furthermore, multidimensional parameters such as temperature rise, median voltage, capacity, power, and strain are used to quantify the SOS. The SOS is a battery state parameter, with its value ranging from 0% to 100%. Experimental results demonstrate that the presented approach can warn of thermal runaway around 5 h in advance.

The development of new energy vehicles is an important step towards carbon neutrality[1,2]. Lithium-ion batteries have become the dominant energy storage solution for electric vehicles owing to their superior energy density and long cycle life[3–5]. However, the fires, explosions, and other safety incidents of batteries are frequent[6–8]. The investigation report shows that thermal runaway is the main cause of battery safety accidents[9,10]. Obviously, the issue of thermal runaway has seriously hindered the further promotion and large-scale application of electric vehicles. Therefore, solutions to this problem are urgently required to pass the last mile for early warning of thermal runaway.

Mechanical, electrical, or thermal abuse can induce thermal runaway, a phenomenon involving an exothermic chain reaction within a cell. This reaction causes a temperature increase of thousands of degrees, ultimately leading to spontaneous combustion[11]. In the early stage of thermal runaway, the electric and thermal behavior of the battery remains unchanged, which has strong concealment[12,13]. In the final stage, the battery may experience an exothermic chain reaction, leading to a rapid temperature rise and eventual explosion. Clearly, the thermal runaway has a strong suddenness[14]. Consequently, it is a challenging issue for early warning of battery thermal runaway.

Currently, the study of the thermal runaway evolution mechanism under different induced conditions has attracted the attention of a wide range of scholars[15]. Mechanical external forces can cause destructive deformation and generate flammable electrolytes, which lead to spontaneous combustion of the battery. Thermal runaway triggered by nail penetration occurs faster than indentation loads. This causes a surge in heat generation and the development of severe internal short circuits[16,17]. Overcharging can accelerate the lithium precipitation reaction and solid electrolyte interface membrane decomposition, which increases the risk of thermal runaway[18]. The heat accumulated within the battery cannot be dissipated, leading to a rise in temperature and a cascade of chain reactions[19,20]. Research has demonstrated that the higher the heating temperature of the battery, the shorter the time required to trigger thermal runaway[21,22]. However, existing thermal runaway mechanism analysis methods based on temperature cannot describe mechanical behaviors such as material deformation, cracking, etc. Meanwhile, this method cannot capture the local effects and nonlinear behaviors of the battery.

Existing thermal runaway warning techniques are mainly based on gas, sound, electrical, and thermal signals[23–25]. Gas sensors can detect gas leakage from the battery and issue an early warning signal. Gas chromatography and Fourier-transform infrared spectroscopy enable the detection of organic vapor composition and concentration during the initial stages of battery thermal runaway. It was reported that the concentration of CO, CO_2, and CH_4 can warn of the overheating and over-charge thermal runaway of 18650 type battery[26–28]. Further, H_2 was captured to detect the growth of lithium dendrites and warn of thermal runaway[29]. It is derived from the redox reactions of the electrolyte or solid electrolyte interface (SEI) under high temperature conditions. Unfortunately, no volatilized gas is present to serve as an early warning signal for thermal runaway under normal operating conditions. Meanwhile, as the gas accumulates inside the battery, the opening of the safety valve or the rupture pouch can emit a shrill acoustic signal. It is evident that artificial intelligence algorithms based on acoustic signals provide early warning of thermal runaway[30,31]. However, acoustic signals are susceptible to interference from ambient noise, posing a challenge for the accurate warning of thermal runaway.

[1]School of Control Science and Engineering, Shandong University, Jinan, China. [2]These authors contributed equally: Xin Gu, Jinglun Li.
✉e-mail: yshang@sdu.edu.cn; zchui@sdu.edu.cn

The electrical and thermal parameters of the battery are important indicators for early warning of thermal runaway[32,33]. The BMS can issue an alarm signal if the predicted external temperature or voltage deviates from the threshold based on models or intelligent algorithms[34,35]. However, the heat generated by internal reactions cannot be rapidly transferred to the surface, making it difficult for external parameters to accurately reflect internal structural damage. Consequently, thermal runaway warning systems based on external parameters experience delays. Fortunately, fiber optic sensors can measure battery internal parameters such as stress and core temperature, which are considered an ideal solution for thermal runaway warning[36–39]. However, the implantation of fiber optic sensors has the following issues: (1) this raises the cost of the battery, which is unacceptable to users. (2) It deteriorates the battery structure, posing a risk to its safety. (3) It is difficult to precisely parse the coupled multi-signal.

European Council for Automotive Research and Development has established an eight-stage battery safety evaluation scheme, where higher stages denote greater risk[40]. A multi-level safety assessment model for batteries was proposed to achieve the thermal runaway risk evolution hierarchical[41,42]. In conclusion, the existing methods can only qualitatively assess the SOS, which leads to a short warning time for thermal runaway. Here, we analyze the strain evolution law during thermal runaway and propose the thermal runaway trigger strain point. Further, a battery evaluation indicator-SOS is quantified to warn of thermal runaway. More importantly, the effectiveness of the presented approach is verified under three operating conditions. The experimental results indicated that this method can accurately warn the thermal runaway.

Results

Evolution trend analysis of thermal runaway under overheating conditions

Figure 1a shows the parameter variation curves of an 80% state of charge (SOC) battery during thermal runaway, which is divided into five stages. Stage I ($\frac{dS}{dt} > 0.01\,\mu \cdot s^{-1}$) is characterized by a temperature range of 30–90 °C, during which the stain emerges in conjunction with temperature variations. The strain and temperature have a high linear correlation, indicating that the change in strain is probably caused by the thermal expansion of the electrode material. This phenomenon is broken during stage II ($\frac{dT}{dt} > 0.0025\,^{\circ}C \cdot s^{-1}, \frac{dS}{dt} < 0.01\mu \cdot s^{-1}$), which indicates a sharp drop in strain. The relaxation of the surface structure probably explains this abnormal behavior due to the initial expansion of the cell. The cell bulge is attributed to gas generation, which originates from the evaporation of the electrolyte solvent and the decomposition of the solid electrolyte interface (SEI) membrane. The reaction equation is as follows.

$$\begin{aligned} Li_2CO_3 &\rightarrow Li_2O + CO_2 \uparrow \\ ROCO_2Li &\rightarrow Li_2CO_3 + R \uparrow \\ ROLi &\rightarrow Li_2O + R \uparrow \end{aligned} \tag{1}$$

where R denotes alkyl or aryl.

The slight jitter of the strain is detected during stage I. The repeated experiments proved the commonness of this phenomenon. Additional gas-producing or exothermic reactions could be a contributing factor. Specifically, the reaction between Li metal in the anode and the electrolyte solvent causes a minimal release of hydrocarbon gases. The reaction equation is as follows.

$$\begin{aligned} 2Li + 2CH_3OCH_3 &\rightarrow CH_3CH_3 \uparrow + H_2 \uparrow + 2LiOCH_3 \\ 2Li + 2CH_3CO_3 &\rightarrow CH_2 = CH_2 \uparrow + 2CO_2 \uparrow + 2LiOH \end{aligned} \tag{2}$$

The curve of stage III ($\frac{dS}{dt} > 0.05\mu \cdot s^{-1}$) is zoomed in Fig. 1b. While the temperature remains constant, the strain shows a continuous upward trend. This indicates that the increase in strain is attributed to battery bulging caused by gas generated from internal reactions, rather than thermal expansion. From a temperature perspective, the system is still in the initial phase of thermal runaway. The separator decomposing and absorbing heat restrained the further increase of the temperature, whose reaction equation was displayed as follows.

$$\begin{aligned} CH_2 - CH_2 &\rightarrow CH_2 = CH_2 \uparrow + H_2 \uparrow \\ CH_2 - CH_2 &\rightarrow CH_3 - CH_3 \uparrow + H_2 \uparrow \\ CH_3 - CH(CH_3) - CH_2 &\rightarrow CH_3 - CH = CH_2 + CH_4 \\ CH_3 - CH(CH_3) - CH_2 &\rightarrow CH_2 = CH - CH_3 + CH_4 \end{aligned} \tag{3}$$

The phenomenon of stage IV ($\frac{dT}{dt} > 0.2^{\circ}C \cdot s^{-1}$) is the exact opposite of stage III, which is zoomed in Fig. 1c. The temperature increased sharply while the strain remained constant. The temperature rise is primarily induced by a violent exothermic reaction. This reaction included the decomposition of the anode active material, partial oxygen release from the cathode, and micro internal short circuits. However, there is no established mechanism to explain the observed strain pattern. Fortunately, we present a hypothesis that the incomplete oxidation of hydrocarbons reduces the volume of gas, whose reaction equations are shown as follows.

$$\begin{cases} CnH_2n + 2 + (n+1)/2O_2 \rightarrow nCO + (n+1)H_2O \\ C_2H_6 + O_2 \rightarrow 2CO + 3H_2O \\ C_2H_6 + 3.5O_2 \rightarrow 2CO_2 + 3H_2O \\ C_2H_6 + 2.5O_2 \rightarrow 2CO + 1CO_2 + 3H_2O \end{cases} \tag{4}$$

In stage V ($\frac{dT}{dt} > 1^{\circ}C \cdot s^{-1}$), the thermal runaway trigger stress point S_{tr} is defined as the knee point in the stress rise process. Thermal runaway occurred abruptly, accompanied by a sharp rise in both temperature and strain. A large amount of gas and heat is generated by internal reaction, which leads to the peak of temperature and strain. A variety of reactions occur at this stage, whose reaction equations are shown as follows.

$$\begin{aligned} LiPF_6 &\rightarrow LiF + PF_5 \\ EC &\rightarrow CO_2 \uparrow + H_2 \uparrow \\ DEC &\rightarrow CO_2 \uparrow + 2H_2 \uparrow \\ LiCoO_2 + EC &\rightarrow LiPF_6 + Co_3O_4 + CO_2 \uparrow \\ LiMn_2O_4 + EC &\rightarrow LiPF_6 + MnO_2 + CO_2 \uparrow \end{aligned} \tag{5}$$

Figure S1 demonstrates the strain and temperature trend for overheating thermal runaway of 100% SOC, and 50% SOC batteries, respectively. It is noteworthy that the trends of temperature and strain changes during thermal runaway are nearly identical under different SOC. This indicates that the proposed mechanism of heating-triggered thermal runaway is scientifically sound. In summary, we conclude that the trend of characteristic parameters changes during thermal abuse-triggered thermal runaway, as shown in Fig. 1.

Table 1 demonstrates the important feature during overheating thermal runaway at different SOC. It is worth noting that the thermal runaway trigger strain S_{tr}, is proposed. As the SOC increases, S_{tr} and maximum strain S_m demonstrate a reduction. The probable reason is that high SOC batteries contain a large amount of electrical energy, and the ohmic heating from short-circuit currents exacerbates the thermal runaway process. This leads to insufficient decomposition reactions of the SEI and separator, which reduces the gas production and lowers the strain. A similar trend was observed for the thermal runaway trigger temperature T_{tr}, and maximum temperature T_m. The time required for thermal runaway decreases with increasing SOC of the battery. This is reasonable because a higher SOC indicates greater lithium intercalation into the graphite anode and increased electrochemical energy storage. In other words, high SOC batteries are more susceptible to thermal runaway. Interestingly, the S_{tr} is on average 906 s earlier than the T_{tr} of different SOC. This observation highlights that the strain signal can predict thermal runaway earlier than temperature.

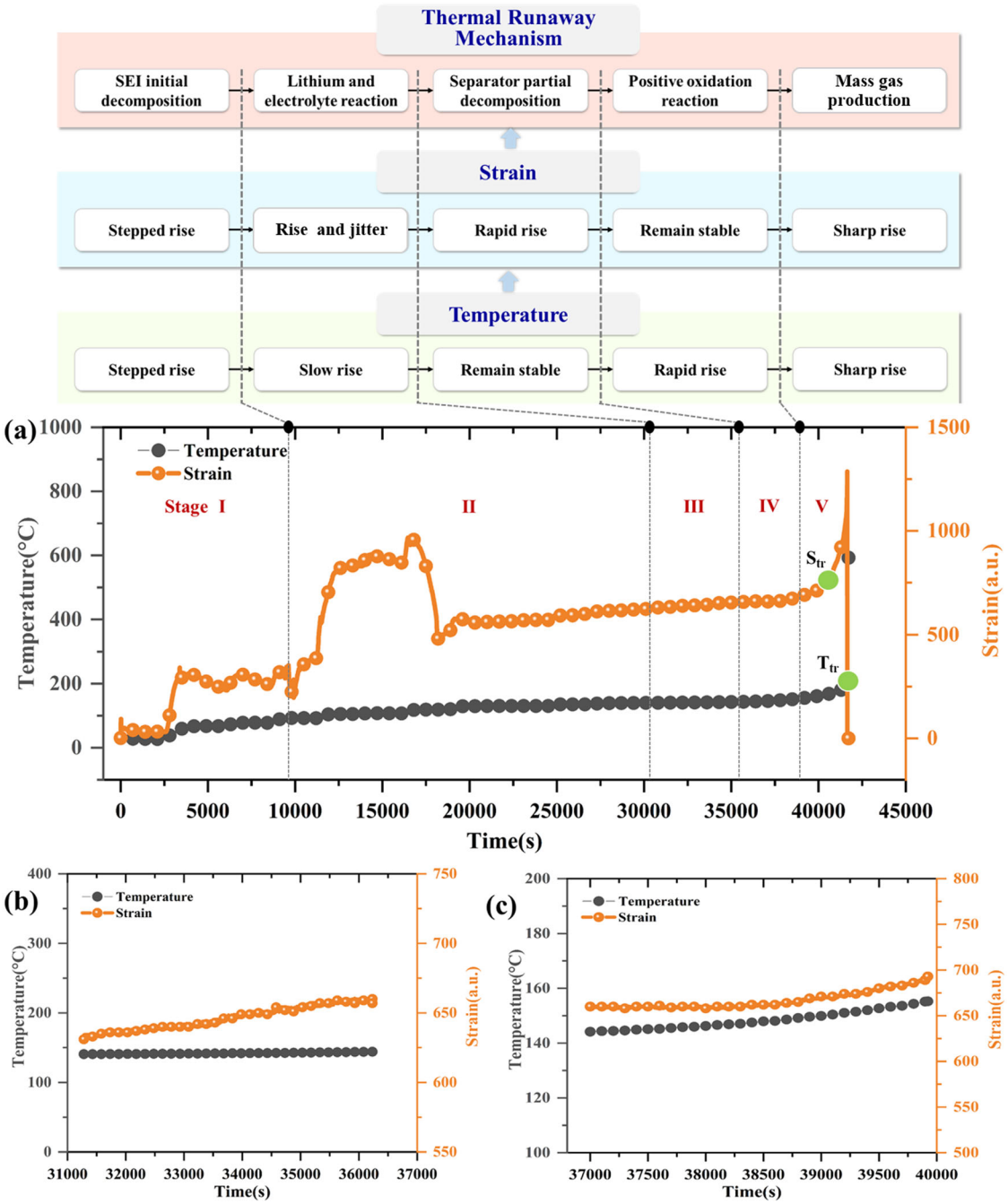

Fig. 1 | The battery parameter variation curves of 80% SOC during thermal runaway. a Strain and temperature curve. **b** Zoomed-in figure of the stage III. **c** Zoom-in figure of the stage IV.

Table 1 | The important feature during overheating thermal runaway at different SOC

Cells	SOC (%)	S_{tr} (10^{-6})	S_m (10^{-6})	$t_{S\text{-}tr}$ (s)	$t_{S\text{-}m}$ (s)	T_{tr} (°C)	T_m (°C)	$t_{T\text{-}tr}$ (s)	$t_{T\text{-}m}$ (s)
1	50	985	1264	41,997	43,367	168	751	43,193	43,449
2	80	724	1266	40,912	41,651	166	671	41,325	41,691
3	100	630	787	20,457	21,793	179	1139	21,568	21,806

Evolution trend analysis of thermal runaway under over-rate conditions

The parameter variation curves of the battery with a charging rate of 3 C are demonstrated in Fig. S2a. As the number of cycles increases, the voltage curve displays morphological variations. The enhanced slopes of voltage rise and fall imply a gradual capacity degradation. It can be observed that the temperature variation pattern remains consistent across multiple charge-discharge cycles: a rise during charging, a slight increase during discharging, and a decline during rest periods. In contrast, the strain evolution exhibits a more complex behavior. At the end of each charging period, the strain peak emerges due to the thickening of the anode material. With increasing cycle numbers, the peak rises substantially, highlighting a growing risk of

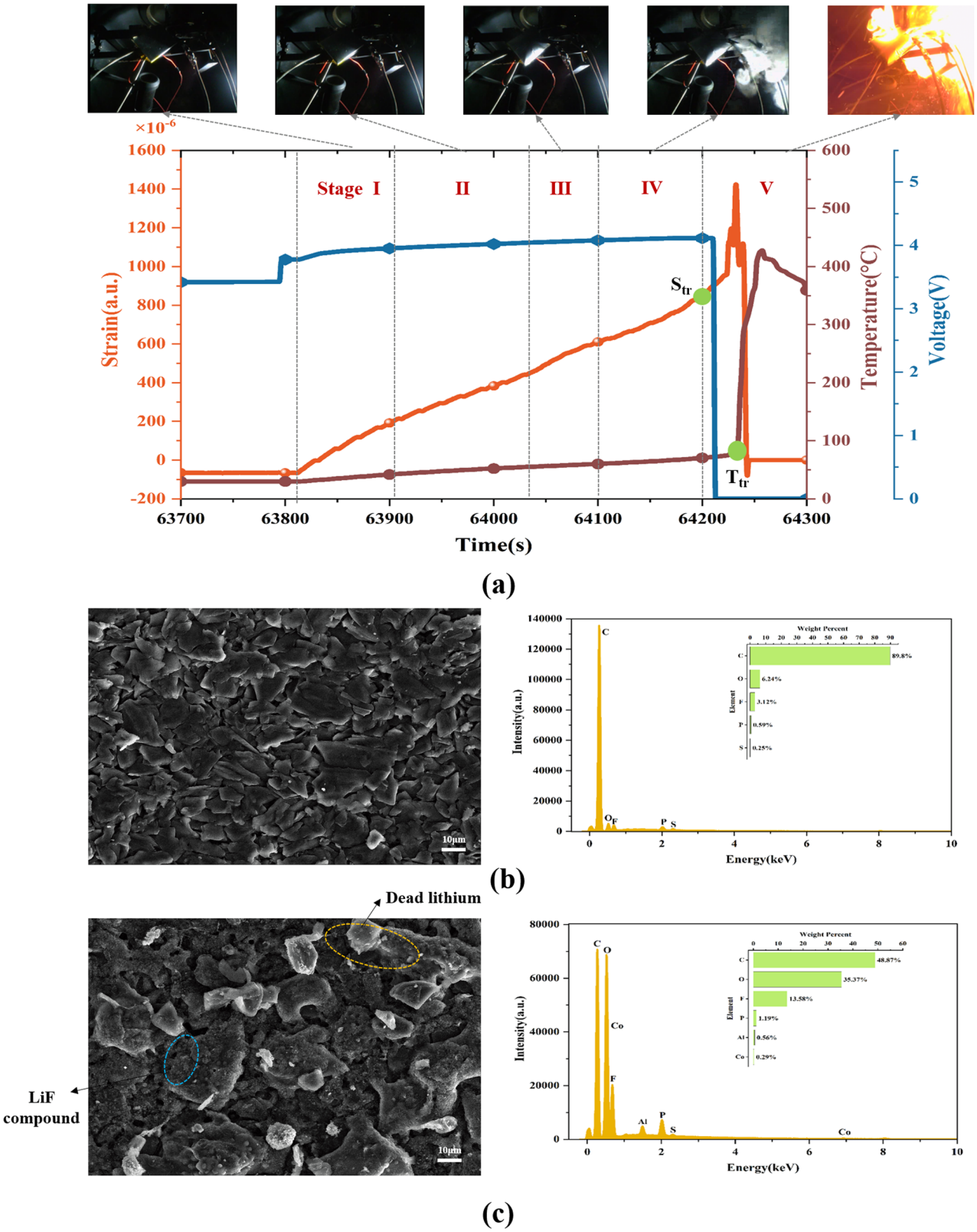

Fig. 2 | The battery parameter variation curves with 3C-rate during thermal runaway. a Strain, temperature, and voltage curves. **b**, **c** The surface morphology and elemental composition of the negative electrode of a new and a thermal runaway battery, respectively.

mechanical rupture. Besides, the lowest strain of each cycle also increased, which reflects the gradually aggravated damage degree of the negative electrode and the non-uniformity of current distribution.

The curves of the final cycle (i.e., thermal runaway) are zoomed in Fig. 2a, which is divided into five stages. Stage I is observed at the beginning of the high-rate charging phase, with a shorter duration compared to the period under overheating conditions. The primary cause is that the high current damages the internal structure of the battery. The stage II indicates that a slow increase of strain and temperature. Ohmic heating is the primary source of the increasing thermal load, driven by the combination of

Table 2 | The important feature during thermal runaway at different over-rate

Cells	Rate	S_{tr} (10^{-6})	S_m (10^{-6})	$t_{S\text{-}tr}$ (s)	$t_{S\text{-}m}$ (s)	T_{tr} (°C)	T_m (°C)	$t_{T\text{-}tr}$ (s)	$t_{T\text{-}m}$ (s)
1	3 C	845	1411	64,200	64,235	89	438	64,233	64,261
2	4 C	203	983	25,961	26,121	71	425	26,132	26,178
3	5 C	193	3877	550	574	64	225	560	564

excessive internal resistance and substantial current flow. Notably, this stage lasted less than 100 s, which is much shorter compared to the overheating trigger condition. The possible reason is that the over-rate depleted the lithium ions on the electrodes, which leads to an increase in internal resistance. In stage III, strain shows an accelerating upward trend. This phenomenon is primarily caused by the internal electrochemical reactions that produce volatile gases. Stage IV demonstrates the phenomenon of continuous increase of strain and temperature. This is attributed to the increase in electrode thickness and a large amount of heat generation caused by high-rate charging. In stage V, the strain and temperature rise rapidly. Compared to the overheating trigger condition, the strain signal appeared earlier than the temperature. The probable explanation is that over-rate charging generates a lot of internal heat, which leads to thermal expansion. Meanwhile, there is a delay for the internal heat to transfer to the surface of the battery.

Figure 2b, c provides the surface morphology and elemental composition of the negative electrode for a new battery and a thermal runaway battery, respectively. Morphological examination of the anode material confirms a smooth and homogeneous surface, with no indications of lithium plating in the initial state. In contrast, post-thermal runaway batteries exhibit an amount of dead lithium on the carbon particles. The increase in the fluorine (F) element serves as a critical indicator of battery thermal runaway, reflecting the decomposition of electrolyte components under elevated temperatures. The formation of dead lithium is primarily caused by high-rate charging, during which lithium ions fail to intercalate efficiently into the carbon layers. This results in their excessive deposition on the surface and subsequent reduction to an atomic state.

Dead lithium is a key factor in the degradation of battery performance and safety, which can cause the risk of short circuits and thermal runaway.

As shown in Fig. S2, the cycle numbers before thermal runaway decrease as the charging rate increases. This phenomenon can be attributed to the excessive heat generated during high-rate charging, which exacerbates battery degradation and increases the risk of thermal runaway. Besides, more drastic strain fluctuations are detected under the higher changing rate. The battery strain at a 5 C charging rate remained stable in the early stage and then suddenly rose. Owing to the limited number of cycles, no parameter anomalies are observed prior to the onset of thermal runaway. The strain curve contains the third and fourth stage phenomena. The battery was charged at a 5 C rate, not one complete charge/discharge cycle. This phenomenon can be attributed to the heat generated by the high current, which triggers the reaction between lithium and the electrolyte, thereby initiating the entire thermal runaway chain reaction.

Table 2 demonstrates the characteristic parameters of thermal runaway at different over-rates. It can be seen that the thermal runaway trigger strain S_{tr}, gradually decreases with the charging multiplier. However, the thermal runaway maximum strain S_m does not show a similar trend. The thermal runaway trigger temperature T_{tr} and the maximum temperature T_m exhibit no clear correlation with the charging rate. Interestingly, the strain trigger time for thermal runaway is earlier than the temperature. This phenomenon demonstrates that strain can warn of thermal runaway.

Evolution trend analysis of thermal runaway under over-charge conditions

The parameter variation curves of the 110% SOC are displayed in Fig. S3. Similar to the over-rate charging conditions, the change in the voltage waveform reflects the decrease in the battery state of health (SOH). However, the temperature variation is more pronounced compared to that observed under over-rate conditions. Temperature peaks consistently occurred during the constant current stage of each cycle, reaching approximately 45 °C in the initial four cycles. The potential difference between electrodes at high SOC resulted in an excessive emigration of lithium ions from the cathode to the anode. During the discharging phase, the loss of lithium ions at the cathode is compensated by the anode, leading to a reduction in the lithium inventory at the anode. From the fifth cycle, the shortage of lithium-ion inhibits the movement of the internal charges. The loss of lithium leads to a decrease in lithium-ion concentration in the electrolyte, increasing the internal resistance of the battery. Hence, a large amount of joule heat is generated to induce the thermal runaway.

It is noteworthy that the strain variation exhibits an irregular pattern. The initial strain, peak strain, and minimum strain show variations for each cycle. This phenomenon is also evidenced by the variation rule of the characteristic parameters at different cut-off SOC represented in Fig. S3. We postulate that the potential cause may be attributed to localized reactions within the battery that result in non-uniform deformation of the casing. This could lead to the strain measurement points experiencing tension or slackness, causing the strain to fluctuate in a stochastic manner. Moreover, a battery with a higher cut-off SOC can trigger thermal runaway in fewer cycles. The underlying reason is that excessive overcharging accelerates the degradation of the lithium-ion repository. Furthermore, the accumulation of dead lithium on the anode elevates the battery's internal resistance, which subsequently increases heat generation during charge-discharge cycles, thereby raising the likelihood of thermal runaway.

The curves of the final cycle (i.e., thermal runaway) are zoomed in Fig. 3. The various stages of thermal runaway are clearly divided in the diagram. In general, the phenomenon of thermal runaway induced by overcharging is analogous to that triggered by overheating. For example, the initial temperature of each stage is lower than that of the overheating. The reason can be attributed to the following three factors. (1) The main heat source originates inside the battery, causing the external temperature measurements to exhibit a time lag. (2) Multiple over-charges cause the SEI film to transition from a stable state dominated by solid-state salts to a metastable state dominated by carbonates, which can not effectively isolate the electrolyte from the negative electrode of the battery. Therefore, the anode can react with the electrolyte at lower temperatures. (3) Overcharging results in increased lithium deposition at the anode and a corresponding accumulation of chemical energy within the battery. Both factors collectively facilitate the reaction occurring at a lower temperature.

Table 3 demonstrates the characteristic parameters of thermal runaway at different over-charge SOC. It is evident that the maximum strain S_m and the trigger strain S_{tr} during thermal runaway progressively increase with higher over-charge SOC. As the over-charge SOC increases, the strain triggering time is progressively reduced. What's more, under three different degrees of over-charge SOC, the thermal runaway strain trigger time is earlier than the temperature by 13 s, 129 s, and 21 s, respectively.

Quantitative assessment results of SOS under over-rate conditions

Figure 4 represents the SOS quantitative evaluation results under the 3C-rate charging condition. The trends of different evaluation indicators with the number of cycles are shown in Fig. 4a. It is evident that the initial SOS of batteries is close to 92%, indicating that no abusive treatments were implemented. Notably, SOH shows a decreasing trend throughout the cycle. In contrast, strain demonstrates an increasing trend during cycling. As a result, the SOS exhibits a gradual decline over the cycle numbers. This suggests that the SOS is not linearly dependent on any single parameter but

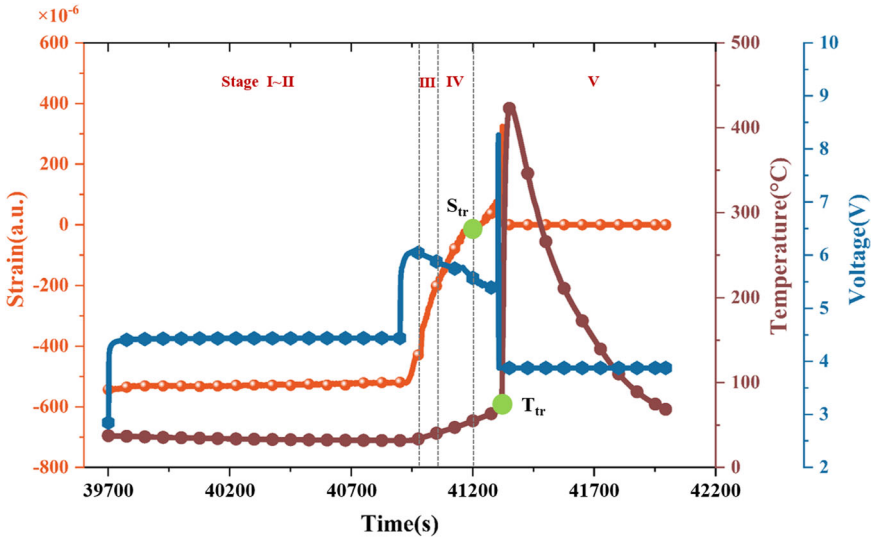

Fig. 3 | The parameter variation curves with 110% SOC over-charge.

rather represents an integrated result shaped by the collective influence of all factors.

Figure 4b illustrates the change pattern of the SOS under over-rate charging. The battery's SOS decreases only 4% over the first four cycles. This suggests that the battery exhibits a certain tolerance to occasional over-rate charging abuse. It's primarily the thickening of SEI films that leads to slight changes in capacity and strain. Unfortunately, the SOS exhibits a sharp reduction of 23% and 29% in the sixth and seventh cycles, respectively. It is evident that a notable increase in surface strain and a decrease in capacity. These indicators indicate that the internal reaction of the anode produces gases that lead to the expansion of the cell volume. This is accompanied by the deterioration of the carbon layer structure. In summary, the SOS trend confirms the thermal runaway mechanism discussed in this paper, which can be applied as a new indicator for early warning of thermal runaway.

As shown in Table 4, the lithium-ion battery experienced thermal runaway after undergoing 8 and 4 complete charge and discharge processes at 3 C and 4 C rates, respectively. This suggests that the severity of structural damage to the battery escalates with higher charging current magnitudes. Taking SOS = 60% as the warning threshold, the proposed method gave an early warning of thermal runaway 2 rounds in advance. Combining the charging time under different working conditions, according to an average of 2.5 h per round, the method proposed in this paper realizes the thermal runaway warning for 5 h.

Quantitative assessment results of the SOS under over-charge conditions

Figure 5 illustrates the pattern of SOS variation for a battery under the 105% SOC over-charge condition. Specifically, Fig. 5a depicts the variation of SOS-related parameters as the number of cycles increases. It is evident that the SOH of the battery exhibits a decline from the first cycle, decreasing from 100% to 81.2%. This decline continues consistently across subsequent cycles, ultimately reaching a critical threshold of 22.5% prior to thermal runaway. Concurrently, other parameters, including median voltage, peak power, charging temperature rise, and strain difference, progressively increase with each cycle. These parameter variations collectively indicate the degradation of the battery's performance, ultimately resulting in a reduction of the SOS.

Figure 5b presents a waterfall chart depicting the degradation of the SOS in each cycle. It is evident that the rate of SOS decline exhibits a progressive acceleration. In particular, the SOS decreased by about 3%, 6%, and 17% in the second, third, and fourth cycles, respectively. Furthermore, the initial over-charge had the most severe impact on the battery's SOS, resulting in a 37% reduction. An alarm was triggered during the second cycle, providing a 5 h advance warning. Table 4 presents the parameter variations under different over-charge SOC. This elucidates the degradation patterns of batteries under cyclic overcharging conditions. When the battery experiences a 125% SOC/130% SOC over-charge condition, the proposed method can detect anomalies and trigger an alarm signal within a single charging cycle.

Comparison with conventional methods

To evaluate the state-of-the-art of the proposed approach, a comparison of the thermal runaway warning times of the different methods is given in Table 5. The voltage-based method can provide 1.47 h early warning of thermal runaway. The temperature-based method can signal a thermal runaway warning 0.57 h. This is because voltage abnormalities (e.g., dips or oscillations) usually occur in the final stages of thermal runaway, when irreversible phenomena such as diaphragm meltdowns and large-scale short circuits have already occurred in the battery. Similarly, the temperature transferring from the internal to the external exhibits hysteresis due to thermal inertia and the thermal resistance of the battery structure. Gas-based and sound-based technologies can give thermal runaway warning signals 0.7 h and 0.3 h in advance, respectively. Potential explanations include the high gas concentration and safety valve rupture acoustic signals typically occur during the thermal runaway outbreak phase. In addition, mechanical vibration, fan operation, and other noises may cover up the acoustic signal of the safety valve. Fortunately, the proposed technique provides an early warning of thermal runaway up to 5 h in advance. This is attributed to the fact that SOS incorporates multi-dimensional battery parameters such as electricity, heat, and force, which can accurately capture abnormal battery behavior.

Discussion

The thermal runaway strain curve is presented under abusive operating conditions such as overheating, over-rate, and over-charge. Generally, it can be divided into five stages. A phenomenon of hydrocarbons' incomplete combustion during thermal runaway has been discovered. Interestingly, we define the thermal runaway trigger stress point. The thermal runaway trigger strain is correlated with the degree of over-rate and over-charge. However, the thermal runaway maximum strain does not exhibit a clear trend. Importantly, the strain signal can warn of thermal runaway earlier than the temperature signal. What's more, we propose a quantitative SOS assessment technique. This can effectively assess battery safety status even when single parameters show no variations. We present the thermal runaway warning technique based on SOS that can signal up to 5 h in advance.

Table 3 | The important feature during thermal runaway at different over-charge

Cells	Over-SOC	S_{tr} (10^{-6})	S_m (10^{-6})	$t_{S\text{-}tr}$ (s)	$t_{S\text{-}m}$ (s)	T_{tr} (°C)	T_m (°C)	$t_{T\text{-}tr}$ (s)	$t_{T\text{-}m}$ (s)
1	110%	65	322	41,262	41325	77	425	41,275	41,340
2	125%	1215	2039	31,534	31661	71	385	31,663	31,720
3	130%	1501	2310	23,158	23278	83	467	23,179	23,281

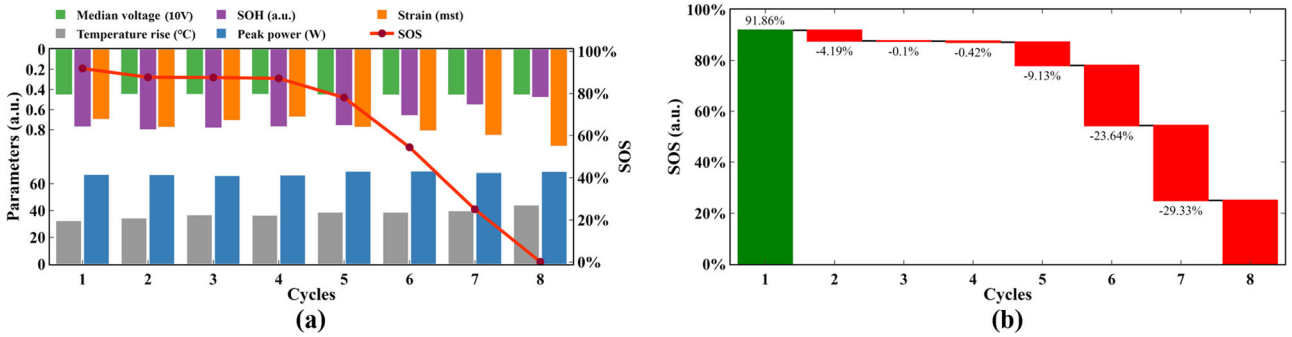

Fig. 4 | SOS quantitative assessment results under 3C-rate conditions. a Evaluation index and SOS change trend. **b** SOS waterfall diagram.

SOS comprehensively considers key parameters such as voltage, temperature, strain, etc., which can effectively prevent the occurrence of battery safety accidents. Moreover, SOS technology can help optimize charging and discharging strategies to avoid operating the battery under extreme conditions, thus extending its service life. More importantly, SOS and other status parameters (e.g., SOC, SOH, SOP, etc.) provide users with comprehensive battery status information. This not only helps to improve the management efficiency of the BMS, but also provides users with accurate battery status feedback. Therefore, SOS technology provides a direction for the intelligent and automated development of BMS.

Methods

The SOS of power batteries is highly susceptible to the coupling effects of working conditions, temperature, mechanical shock, aging, and other factors. Firstly, the evaluation indices such as temperature rise, median voltage, capacity, power, and strain are determined. Then, the above indicators are normalized to a standard scale and assigned specific weighting coefficients.

Finally, the weighted Euclidean distance between each indicator and the optimal/worst values is determined to achieve the quantitative assessment of SOS and the advanced warning of thermal runaway.

An evaluation matrix A is constructed based on multiple evaluation indicators.

$$A = \begin{bmatrix} T_{11} & T_{12} & \cdots & T_{1m} \\ V_{21} & V_{22} & \cdots & V_{2m} \\ \vdots & \vdots & \ddots & \vdots \\ S_{n1} & S_{n2} & \cdots & S_{nm} \end{bmatrix} \quad (6)$$

Table 4 | The important feature of SOS at different working conditions

Cells	Rate	Cycles	Warning time (h)	Cells	SOC (%)	Cycles	Warning time (h)
1	3 C	8	5.0	3	105	4	5.0
2	4 C	4	5.0	4	110	3	2.5
-	-	-	-	5	125	1	2.5
-	-	-	-	6	130	1	2.5

where T, V, and S are the temperature, voltage, and strain of the battery, respectively, m represents the total number of evaluation indicators, and n is the number of cells.

To ensure scale consistency among the indicators, the evaluation matrix should undergo normalization. The transformation of negative indicators into positive indicators of the same magnitude is required to construct the normalization matrix E.

$$E = \begin{bmatrix} e_{11} & e_{12} & \cdots & e_{1m} \\ e_{21} & e_{22} & \cdots & e_{2m} \\ \vdots & \vdots & \ddots & \vdots \\ e_{n1} & e_{n2} & \cdots & e_{nm} \end{bmatrix} \quad (7)$$

where e_{nm} denotes the normalization indicator values.

The optimal D^+ and worst D^- solutions for each indicator are determined.

$$D^+ = (D_1^+, D_2^+, \cdots D_m^+) = (\max\{e_{11}, e_{21}, \cdots e_{n1}\}, \cdots \max\{e_{1m}, e_{2m}, \cdots e_{nm}\}) \quad (8)$$

$$D^- = (D_1^-, D_2^-, \cdots D_m^-) = (\min\{e_{11}, e_{21}, \cdots e_{n1}\}, \cdots \min\{e_{1m}, e_{2m}, \cdots e_{nm}\}) \quad (9)$$

The weighted distance of each metric from the optimal/worst solution is calculated.

$$d_i^+ = \sqrt{\sum_{j=1}^{m} (\omega_j \times D_j^+ - \omega_j \times D_{ij})^2} \quad (10)$$

$$d_i^- = \sqrt{\sum_{j=1}^{m} (\omega_j \times D_j^- - \omega_j \times D_{ij})^2} \quad (11)$$

The battery SOS is quantitatively assessed.

$$SOS = \frac{\sqrt{\sum_{j=1}^{m} (w_j \times x_{ij} - w_j \times x_j^{\min})^2}}{\sqrt{\sum_{j=1}^{m} (w_j \times x_{ij} - w_j \times x_j^{\min})^2} + \sqrt{\sum_{j=1}^{m} (w_j \times x_{ij} - w_j \times x_j^{\max})^2}} \times 100\% (0 \le SOS \le 100\%) \quad (12)$$

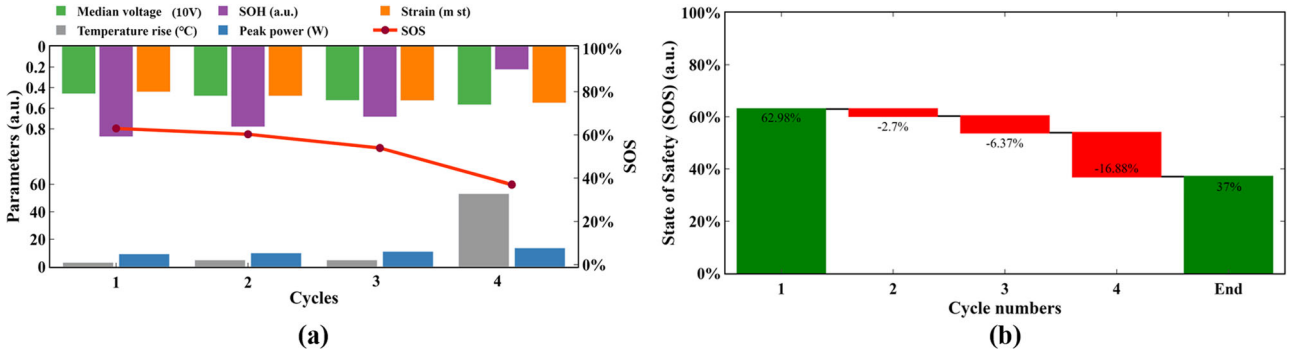

Fig. 5 | SOS quantitative assessment results under 105% SOC over-charge conditions. a Evaluation index and the SOS change trend. **b** SOS waterfall diagram.

Table 5 | Comparison with existing methods

Methods	Voltage-based	Temperature-based	Gas-based	Sound-based	Proposed method
Time	1.47 h	0.57 h	0.7 h	0.3 h	5 h

The greater the SOS, the higher the battery safety and the more stable its operational state. The smaller the SOS, the higher the risk of battery instability and the greater the chance of safety hazards.

Overheating test protocol

The tested $LiCoO_2$ battery had a nominal capacity of 3.9 Ah and upper/lower cutoff voltages of 2.8 V/ 4.4 V, respectively. The accelerating rate calorimeter (ARC) was set in the heating-waiting-seeking mode during the test. The battery will be heated up for about 5 °C before entering the waiting period. The temperature inside the cavity will track the battery during the waiting period for 30 min. Then, the battery temperature is considered stable. After that, the temperature rising rate will be observed during the seeking period, which can indicate the self-heating of the battery. The over-heating test ended when the temperature of the battery surface reached 300 °C or the temperature rise exceeded 0.1 °C/min.

Over-rate test protocol

The over-rate thermal runaway experiments were carried out inside the ARC. The batteries were charged to cut off voltages in a constant current-constant voltage manner. The changing current rate was set to 3C/4C5/C. The discharge current rate was 1 C. The battery experienced thermal runaway after cycle charge/discharge testing.

Over-charge test protocol

The over-charge thermal runaway experiments were also carried out inside the ARC. The batteries were charged to various pre-set cut-off SOC by the standard const current manner, the final voltage of which was above the nominal max voltage (4.4 V). After a short rest, the batteries were discharged to the lower cut-off voltage (2.8 V). The battery experienced thermal runaway after cycle charge/discharge testing.

Data availability

The datasets generated during and/or analyzed during the current study are available from the corresponding author on reasonable request.

Code availability

Code for the work is available from the corresponding authors upon request.

Received: 24 October 2024; Accepted: 29 May 2025;
Published online: 10 June 2025

References

1. Deng, J., Bae, C., Marcicki, J., Masias, A. & Miller, T. Safety modelling and testing of lithium-ion batteries in electrified vehicles. *Nat. Energy* **3**, 261–266 (2018).
2. Harper, G. et al. Recycling lithium-ion batteries from electric vehicles. *Nature* **575**, 75–86 (2019).
3. Castelvecchi, D. Electric cars: the battery challenge. *Nature* **596**, 336–339 (2021).
4. Ebner, M., Marone, F., Stampanoni, M. & Wood, V. Visualization and quantification of electrochemical and mechanical degradation in Li-ion batteries. *Science* **342**, 716–720 (2013).
5. Wang, F. et al. Physics-informed neural network for lithium-ion battery degradation stable modeling and prognosis. *Nat. Commun.* **15**, 4332 (2024).
6. Miao, Y., Liu, L., Zhang, Y., Tan, Q. & Li, J. An overview of global power lithium-ion batteries and associated critical metal recycling. *J. Hazard. Mater.* **425**, 127900 (2022).
7. Shaffer, B., Auffhammer, M. & Samaras, C. Make electric vehicles lighter to maximize climate and safety benefits. *Nature* **598**, 254–256 (2021).
8. Wu, H., Zhuo, D., Kong, D. & Cui, Y. Improving battery safety by early detection of internal shorting with a bifunctional separator. *Nat.Commun.* **5**, 1–6 (2014).
9. Feng, X., Ren, D., He, X. & Ouyang, M. Mitigating thermal runaway of lithium-ion batteries. *Joule* **4**, 743–770 (2020).
10. Liu, X. et al. Thermal runaway of lithium-ion batteries without internal short circuit. *Joule* **2**, 2047–2064 (2018).
11. Finegan, D. P. et al. The application of data-driven methods and physics-based learning for improving battery safety. *Joule* **5**, 316–329 (2021).
12. Gu, X. et al. An Early minor-fault diagnosis method for lithium-ion battery packs based on unsupervised learning. *IEEE/CAA J. Autom. Sin.* **10**, 810–812 (2023).
13. Shang, Y. et al. A multi-fault diagnosis method based on modified sample entropy for lithium-ion battery strings. *J. Power Sources* **446**, 227275 (2020).
14. Liu, K. et al. To wards long lifetime battery: AI-based manufacturing and management. *IEEE/CAA J. Autom. Sin.* **9**, 1139–1165 (2022).
15. Feng, X. et al. Thermal runaway mechanism of lithium ion battery for electric vehicles: a review. *Energy Storage Mater* **10**, 246–267 (2018).
16. Li, H., Zhou, D., Zhang, M., Liu, B. & Zhang, C. Multi-field interpretation of internal short circuit and thermal runaway behavior for lithium-ion batteries under mechanical abuse. *Energy* **263**, 126027 (2023).
17. Zhao, R., Liu, J. & Gu, J. Simulation and experimental study on lithium ion battery short circuit. *Appl. Energy* **173**, 29–39 (2016).
18. Liu, J., Wang, Z., Bai, J., Gao, T. & Mao, N. Heat generation and thermal runaway mechanisms induced by overcharging of aged lithium-ion battery. *Appl. Thermal Eng.* **212**, 118565 (2022).

19. Mao, N., Zhang, T., Wang, Z. & Cai, Q. A systematic investigation of internal physical and chemical changes of lithium-ion batteries during overcharge. *J. Power Sources* **518**, (2022).
20. Guo, R., Lu, L., Ouyang, M. & Feng, X. Mechanism of the entire overdischarge process and overdischarge-induced internal short circuit in lithium-ion batteries. *Sci. Rep.* **6**, 30248 (2016).
21. He, T. et al. An investigation on thermal runaway behaviour of a cylindrical lithium-ion battery under different states of charge based on thermal tests and a three-dimensional thermal runaway model. *J Clean. Prod.* **388**, 135980 (2023).
22. Ren, D. et al. Investigating the relationship between internal short circuit and thermal runaway of lithium-ion batteries under thermal abuse condition. *Energy Storage Mater.* **34**, 563–573 (2021).
23. Chen, J. et al. Investigating the thermal runaway features of lithium-ion batteries using a thermal resistance network model. *Appl. Energy* **295**, 117038 (2021).
24. Zhang, L., Zhao, P., Xu, M. & Wang, X. Computational identification of the safety regime of Li-ion battery thermal runaway. *Appl. Energy* **261**, 114440 (2020).
25. Zhang, X. et al. A critical review of thermal runaway prediction and early-warning methods for lithium-ion batteries. *Energy Mater. Adv.* **4**, 0008 (2023).
26. Zhang, Q. et al. Research on the effect of thermal runaway gas components and explosion limits of lithium-ion batteries under different charge states. *J. Energy Storage* **45**, 103759 (2022).
27. Fernandes, Y., Bry, A. & de Persis, S. Identification and quantification of gases emitted during abuse tests by overcharge of a commercial Li-ion battery. *J. Power Sources* **389**, 106–119 (2018).
28. Cummings, S. R. et al. Systems and methods for monitoring for a gas analyte. U.S. Patent 10877011 (2020).
29. Jin, Y. et al. Detection of micro-scale Li dendrite via H_2 gas capture for early safety warning. *Joule* **4**, 1714–1729 (2020).
30. Lyu, N. et al. Fault warning and location in battery energy storage systems via venting acoustic signal. *IEEE J. Emerg. Sel. Topics Power Electron.* **11**, 100–108 (2021).
31. Su, T., Lyu, N., Zhao, Z., Wang, H. & Jin, Y. Safety warning of lithium-ion battery energy storage station via venting acoustic signal detection for grid application. *J. Energy Storage* **38**, 102498 (2021).
32. Liu, K., Shang, Y., Ouyang, Q. & Widanage, W. D. A data-driven approach with uncertainty quantification for predicting future capacities and remaining useful life of lithium-ion battery. *IEEE Transac. Industrial Electron.* **68**, 3170–3180 (2021).
33. Shah, K., Chalise, D. & Jain, A. Experimental and theoretical analysis of a method to predict thermal runaway in Li-ion cells. *J. Power Sources* **330**, 167–174 (2016).
34. Zhou, Z., Li, M., Zhou, X., Ju, X. & Yang, L. Investigating thermal runaway characteristics and trigger mechanism of the parallel lithium-ion battery. *Appl. Energy* **349**, 121690 (2023).
35. An, Z., Shah, K., Jia, L. & Ma, Y. Modeling and analysis of thermal runaway in Li-ion cell. *Appl. Thermal Eng.* **160**, 113960 (2019).
36. Mei, W. et al. Operando monitoring of thermal runaway in commercial lithium-ion cells via advanced lab-on-fiber technologies. *Nat. Commun.* **14**, 5251 (2023).
37. Battery2030+ Research Initiative: Large-scale, long-term European research roadmap for batteries. European Commission. (accessed 1 Feb 2023); https://battery2030.eu/.
38. Miele, E. et al. Hollow-core optical fibre sensors for operando Raman spectroscopy investigation of Li-ion battery liquid electrolytes. *Nat. Commun.* **13**, 1651 (2022).
39. Yu, Y. et al. Real-time monitoring of internal structural deformation and thermal events in lithium-ion cell via embedded distributed optical fibre. *J. Power Sources* **521**, 230957 (2022).
40. Josefowitz, W. et al. Assessment and testing of advanced energy storage systems for propulsion European testing report. In *Proc. of the 21*st *Worldwide Battery, Hybrid and Fuel Cell Electric Vehicle Symposium & Exhibition, EVS 21* (EU, Monaco, 2005).
41. Wang, J. et al. Multiparameter warning of lithium-ion battery overcharge-thermal runaway. *J. Energy Storage* **78**, 110088 (2024).
42. Cabrera-Castillo, E., Niedermeier, F. & Jossen, A. Calculation of the state of safety (SOS) for lithium ion batteries. *J. Power Sources* **324**, 509–520 (2016).

Acknowledgements

This work was supported by the National Natural Science Foundation of China (No. 62333013, U24A20159, and 62173211) and the Natural Science Foundation of Shandong Province, China (No. ZR2021JQ25).

Author contributions

X.G. conceived the original idea of available capacity estimation, designed the research, and wrote the initial draft of the manuscript. The experimental studies were performed by X.G., Y.S., J.L. and Y.Z. The computational studies were performed by X.G., X.T., H.G. and Z.Z. Y.S., C.Z. led and supervised the project, participated in paper writing and revision, and provided guidance to all co-authors. All authors discussed the results and commented on the manuscript.

Competing interests

The authors declare no competing interests.

Additional information

Supplementary information The online version contains supplementary material available at https://doi.org/10.1038/s44172-025-00442-1.

Correspondence and requests for materials should be addressed to Yunlong Shang or Chenghui Zhang.

Peer review information *Communications Engineering* thanks Chong Zhu and Zhongbao Wei for their contribution to the peer review of this work.